1

Microstructure and Properties of Engineering Materials

Helmut Clemens, Svea Mayer, and Christina Scheu

1.1 Introduction

In general, engineering materials are grouped into four basic classifications: metals, ceramics, polymers, and semiconductors. While semiconductors represent exclusively functional materials, the remaining three – depending on their application – can be assigned to the group of either structural or functional materials. Independent of the group they belong to, the important properties of solid materials depend on the geometrical atomic arrangement and also the type of bonding that exists between the constituent atoms. The three types of primary or chemical bonds that are found in engineering materials – covalent, ionic, and metallic – and the main contributions to the individual groups are shown in Figure 1.1. Metals and their alloys possess primarily metallic bonding; semiconductors have mainly covalent bonds, whereas many ceramics exhibit a mixture of covalent and ionic bonding. In engineering polymers, weak secondary forces of attraction (van der Waals forces) exist between the extended covalently bound hydrocarbon chains (Figure 1.1). In general, the nature of bonding depends on the electronic structure of the constituent atoms forming the solid and arises from the tendency of atoms to obtain stable electron configurations.

The structure of engineering materials relates to the arrangement of its internal components. On an atomic level, a structure is understood as the organization of atoms relative to each other. In crystalline materials, the atoms are arranged in periodically repeating arrays which are termed crystal or lattice structures. Metals, for instance, have particularly simple crystal structures: (i) face-centered cubic (fcc), (ii) body-centered cubic (bcc), (iii) hexagonal closed-packed (hcp), and (iv) tetragonal. Many metals and their alloys exist in more than one crystal structure depending on the temperature and composition, but, in most cases, transitions are between these four crystal structures. In contrast, semiconductors usually crystallize either in the diamond structure (silicon, germanium) or often in the zincblende structure (e.g., gallium arsenide).

The next larger structural level is the microscopic level. Here, large groups of atomic arrangements are considered as components of the microstructure, which determines most of the properties of the material. The microstructure of engineering materials is described by the grain size, types of phases present, and description of their structure, shape, and size distributions. In addition, two-dimensional defects such as grain boundaries and heterophase interfaces, one-dimensional defects such as dislocations,

Neutrons and Synchrotron Radiation in Engineering Materials Science: From Fundamentals to Applications, Second Edition. Edited by Peter Staron, Andreas Schreyer, Helmut Clemens, and Svea Mayer.

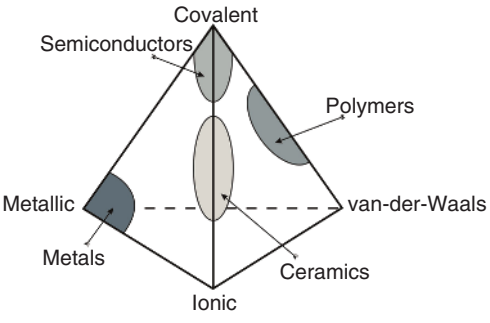

Figure 1.1 Bonding behavior present in different groups of engineering materials. (After [1].) Covalent, ionic, and metallic bonds represent strong primary bonds, whereas van der Waals attraction is a weak secondary bond.

Table 1.1 Influence of atomic arrangement and microstructure on the properties of engineering metallic materials.

Property	Influence of atomic arrangements and atomic defects	Influence of microstructure
Mechanical (e.g., strength and ductility)	Strong	Strong
Electrical, magnetic, and thermal (e.g., resistivity, magnetization, conductivity)	Moderate to strong	Slight to strong
Chemical (e.g., corrosive resistance, catalytic potential)	Slight	Slight to moderate

Control of the atomic arrangement and the microstructure is possible through processes such as casting, powder metallurgy, working, and heat treatment.
Source: Verhoeven 1994 [2]. Reproduced with permission of Wiley.

and zero-dimensional defects such as point defects are important microstructural features that often control the resulting properties.

In this introductory chapter, the microstructure of engineering materials is explained with focus on structural metallic materials, showing a polycrystalline multiphase assembly. The most important microstructure parameters are presented and their influence on mechanical properties is briefly discussed. Table 1.1 roughly summarizes the influence of atomic arrangement, atomic defects, and microstructure upon the properties of metallic materials. In addition, the most important methods for microstructural characterization on a nanometer and micrometer scale will be outlined in this chapter with emphasis on analytical electron microscopy. At the end of the chapter, a selection of textbooks and journal articles is listed, which might be helpful for the reader to deepen his/her understanding of the microstructure and properties of engineering materials [1–15] as well as of methods used for microstructural characterization [7, 16–23].

1.2 Microstructure

Figure 1.2 shows schematically the microstructure of a polycrystalline multiphase metallic material. For a comprehensive and better understanding of the following explanations, Table 1.2 lists the typical mole fractions and size ranges of the individual

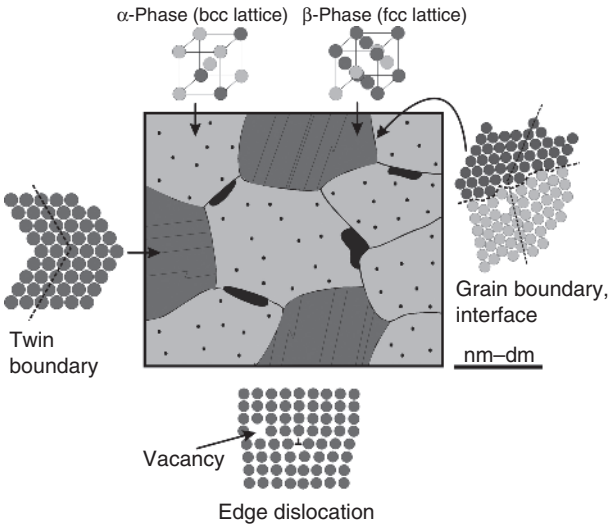

Figure 1.2 Schematic microstructure of a polycrystalline multiphase metallic material. The microstructure consists of α and β grains showing bcc and fcc crystal structures. Within the grains the existence of atomic defects is indicated (vacancies, dislocations, twin boundaries). The grains are separated by grain (phase) boundaries. On some grain boundaries large precipitates are visible. Within one type of grains nanometer-sized particles are present. For further explanations see text and refer to Tables 1.2 and 1.3.

Table 1.2 Microstructure of engineering metallic materials: constituents and their concentration and size ranges.

Microstructural constituents	Range
Vacancies	Equilibrium concentration (mole fraction): 10^{-15} (room temperature) to 10^{-4} (near the melting point)
Dislocations	Density[a]: 10^{10} (annealed) to 10^{16} m^{-2} (heavily cold-worked)
Grains	Size: nm – dm
Subgrains/domains	Size: nm – μm
Alloying elements	Concentration (mole fraction): ppm – 50%
Second phases	Volume fraction: 0 – 70%
Particles (precipitates, dispersoids)	Size: nm – μm; volume fraction: 0 – 70%

a) Dislocation density: the number of dislocations that intersect a unit area of a random surface section; alternatively: the total dislocation length per unit volume of material.

microstructural features and Table 1.3 describes their most important characteristics and their influence on various properties.

The schematic microstructure shown in Figure 1.2 consists of grains of two different phases. The phases differ in their crystal structures (fcc and bcc) and their chemical compositions. As indicated in the depicted crystal structures, each phase forms a solid solution. A solid solution represents a homogeneous crystalline phase that contains two

Table 1.3 The role of microstructural constituents in engineering metallic materials.

Microstructural constituents	Dependent on/characteristics (selection)	Responsible for (examples)
Vacancies	Temperature, deformation	Hardening at low temperatures; diffusion processes at elevated temperatures; diffusional creep
Dislocations	Deformation, temperature, recovery and recrystallization processes; at elevated temperatures edge dislocations may climb, and leave their slip planes	Plastic deformation; strength is controlled by their number and motion; driving force for recrystallization; dislocation creep
Stacking faults	Crystal structure, alloying	Mobility of dislocations, for example, climb of edge dislocations and cross-slip of screw dislocations is hampered
Mechanical twins	Stacking fault energy, deformation, temperature	Additional deformation mechanism at low temperatures and/or high strain rates
Subgrains/domains	Deformation, temperature, stacking fault energy/ordered crystal structure; antiphase boundary energy	Work hardening, creep, creation of antiphase boundaries
Grain boundaries	Lattice orientation between neighboring grains; subdivision in small-angle, medium-angle and high-angle grain boundaries	Work hardening by acting as barriers to slip from one grain to the next; segregation site of impurity atoms
Phase boundaries	Alloy system, composition, phase stability at elevated temperatures	Strengthening effects, for example, in duplex or multiphase steels
Grains	Alloy system, type of nucleation, processing, deformation, heat treatment, recrystallization	Strengthening (see grain boundaries) but ductility is maintained; grain boundary sliding at elevated temperatures (creep, superplasticity)
Annealing twins	Stacking fault energy; characteristic of face-centered cubic materials exhibiting a low stacking fault energy	Lowering of total boundary energy during grain growth
Precipitates/ dispersoids	Alloy system, composition, heat treatment, processing; the interface between particle and matrix can be coherent, semicoherent, or incoherent	Increase in strength by the interaction of moving dislocation; dislocations can loop, cut through or cross-slip the particles at ambient temperatures; at elevated temperatures the dislocations can surmount the particles by climb processes
Phase arrangement (e.g., eutectics, duplex, dual phase)	Alloy system, composition, processing, heat treatment	Positive: control of mechanical and thermo-physical properties; negative: embrittlement in case of brittle phases situated at grain boundaries

or more chemical species. Both substitutional and interstitial solid solutions are possible, such as nickel and chromium in iron (e.g., austenitic steels) and carbon in iron (e.g., heat treatable steels), respectively. The solubility of a metal i.e, its alloying behavior, depends on the atomic size factor (difference in size between solute and solvent atom), the electrochemical effect (the higher the difference in electronegativity, the higher the tendency for the elements to form intermetallic phases rather than extensive solid solutions), and the relative electron valency (a metal of higher electron valency is more likely to dissolve to a large extent in one of lower electron valency than vice versa).

1.2.1 Crystal Defects

The grains in a microstructure represent individual crystals within the polycrystalline material (Figure 1.2). Within each grain, atoms are regularly arranged according to the basic crystal structure but a variety of imperfections, termed crystal defects, may also occur. These defects are point defects (vacancies, interstitial atoms), line defects (dislocations), planar defects (stacking faults, twin boundaries), and volume defects (voids, cavities). Of particular interest are dislocations, because plastic deformation mainly corresponds to the motion of dislocation in response to an applied shear stress (see Chapters 17 and 18). In contrast, hindering of dislocation movement is the basic concept of all strengthening mechanisms (see Section 1.3). Dislocations are subdivided into edge and screw dislocations. At temperatures where no thermally activated diffusion processes take place edge dislocations are confined to their slip planes, whereas screw dislocations can change their slip planes rather easily by cross-slip processes. A schematic drawing of an edge dislocation is shown in Figure 1.2. An edge dislocation is a linear crystalline defect associated with the lattice distortion produced in the vicinity of the end of an extra half-plane of atoms within a crystal. Depending on processing history and/or mechanical loading, subgrains or cell structure, separated by dislocation networks or tangles, can be formed within the grains. In grains showing an ordered crystal structure (e.g., intermetallic phases) domain structures may appear. The individual domains are separated by antiphase boundaries. The corresponding energy is referred to as antiphase boundary energy.

1.2.2 Grain (Phase) Boundaries and Twins

The size of the grains depends on materials processing and heat treatments and can be adjusted in a wide range. In most technically relevant structural metallic materials, such as steels, aluminum alloys, and titanium alloys, the grain size is in the range of several ten micrometers. In contrast, in nanostructured functional materials, for example, superhard coatings with high wear resistance, a grain size in the range of few nanometers is required. The grains as shown in Figure 1.2 are separated by grain (phase) boundaries. In general, grain (phase) boundaries are interfaces that separate two adjoining grains (phases) having different crystallographic orientations and, in the case of phases, different crystal structures and/or chemical compositions. Within the boundary region, which can have a width of one to several atomic distances, an atomic mismatch due to the transition from the crystalline orientation of one grain to that of an adjacent one can occur. Depending on the structure, one can distinguish between high-angle grain boundaries, small-angle grain boundaries, and so on. Since the atoms are differently coordinated and/or bonded along grain boundaries, there is an interfacial or

grain boundary energy associated with them. The magnitude of this energy is a function of the degree of misorientation between the grains, being larger for high-angle grain boundaries although some energy cusps can occur for special grain boundaries. Simple small-angle grain boundaries can be described by dislocation arrangements. A twin boundary as shown in Figure 1.2 is a special type of grain boundary. Atoms of one side of the boundary are located in mirror image positions of the atoms of the other side. Twins result from atomic displacements that are produced from an external stress state (mechanical or deformation twins) and also during annealing heat treatments subsequent to deformation (annealing twins). The formation of twins is closely related to the stacking fault energy of the material. In general, low stacking fault energy facilitates twinning as can be seen in the high density of annealing twins in fcc metals and their alloys, such as copper, α-brass, and austenitic steels. The positive effect of deformation twinning on strain hardening and deformability, for example, is exploited in TWIP (twinning-induced plasticity) steels.

1.2.3 Precipitates and Dispersions

In many structural engineering metal materials precipitates occur. In Figure 1.2 two types of precipitates are drawn schematically: few large ones at grain boundaries and a large number of small particles homogeneously dispersed within individual grains. In many alloys, for example, steels or nickel-based alloys, these precipitates are carbides or intermetallic phases. Their influence on mechanical properties primarily depends on volume fraction, size, distribution, type of precipitate, and arrangement in the microstructure. Large precipitates along grain boundaries as shown in Figure 1.2 can either have a positive or negative effect on the properties. For example, in nickel-based superalloys, precipitates are generated at grain boundaries by means of a special heat treatment in order to minimize grain boundary sliding at high service temperatures. However, such a phase arrangement can also lead to serious embrittlement as observed in steels containing nonmetallic inclusions or cementite films along grain boundaries. Nanometer-sized particles of a second phase, which are uniformly dispersed within the grains, provide the most versatile strengthening mechanism for metallic materials in addition to solid solution strengthening (see Section 1.3). There are different ways to produce extremely fine particles in a metallic matrix: a variety of metallic alloy systems have been developed for which so-called precipitation heat treatments are employed to precipitate a new phase from a supersaturated solid solution. Examples of engineering alloys that are hardened by precipitation treatments include aluminum–copper (e.g., Duraluminum or Dural), nickel–aluminum (e.g., nickel-based superalloys), and some ferrous alloys (e.g., maraging and tool steels). A common feature of these nanometer-sized particles, which usually precipitate in the form of metastable phases, is their coherency with the matrix in the early stages of precipitation. However, during exposure at service temperatures these particles may change their chemistry and are prone to coarsening. Very often this process is accompanied by loss of coherency; thus, a semicoherent or an incoherent interface between particle and matrix is formed. As a consequence the initial hardening mechanism is altered, leading to a decrease in strength.

Another way to strengthen metals and their alloys is to produce a uniform dispersion of several volume fractions of extremely small particles of a very hard and inert

material. The dispersed phase may be either metallic or nonmetallic and they usually do not show coherency with the matrix. Examples are oxide dispersion strengthened (ODS) superalloys: hard nanometer-sized Y_2O_3 particles are mechanically alloyed into the matrix powder and consolidated and processed by powder metallurgical techniques. The dispersion-strengthening effect is often technologically more difficult to realize, however, the strengthening effect is retained at elevated temperatures and for extended service times. This is a direct effect of the inertness of the extremely fine particles, leading to a high resistance against particle growth and re-dissolution effects.

The previous explanation was focused on the various microstructural constituents that range from atomic dimensions to the mesoscopic scale. In engineering metallic materials these constituents appear in a great variety of arrangements that in turn determine many of their properties (Tables 1.1–1.3). In Figure 1.3 a schematic drawing of different microstructures is given along with references to structural metallic materials that are widely used. For completeness it should be mentioned that metals and their alloys that have undergone a severe amount of deformation, as in rolling, forging, or wire drawing, will develop a preferred orientation or deformation texture, in which certain crystallographic planes within the deformed grains tend to align themselves in a preferred manner with respect to the direction of maximum strain. A recrystallization heat treatment, conducted on a cold-worked metal, can produce a preferred orientation

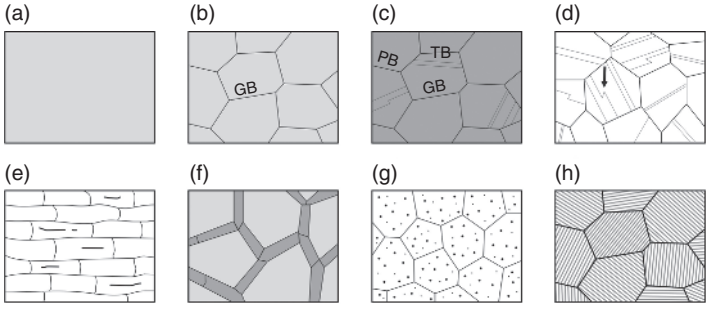

Figure 1.3 Schematic drawings of different microstructures: (a) single crystal: crystalline solid for which the periodic and repeated atomic pattern extends throughout the entire sample without interruption. The properties depend strongly on the orientation of the crystal. Example: single-crystal made of nickel-based superalloys. (b) Polycrystalline single-phase material. The individual grains differ in their crystallographic orientations and are separated by grain boundaries (GBs). Example: α-iron (ferrite) with body-centered cubic (bcc) lattice structure. (c) Two-phase material. The phases differ in chemical composition and crystal structure. The grains are separated either by phase boundaries (PBs) or GBs. One phase, most probably a phase possessing a face-centered cubic (fcc) lattice structure, shows the appearance of annealing twins. TB denotes a coherent twin boundary. Example: α + β-brass, consisting of α-grains (fcc) and β-grains (bcc). (d) Single-phase material exhibiting a large number of annealing twins; arrow: incoherent TB. Example: α-brass (fcc), austenitic stainless steel. (e) Deformed grains with elongated inclusions. Example: ferritic steel with nonmetallic inclusions after rolling to sheet. Due to rolling, the sheet can exhibit a marked texture that may be reflected in anisotropic mechanical properties. (f) Two-phase material, where one of the phases is situated along GBs. Example: pearlitic steel with proeutectoid ferrite on GBs. (g) Polycrystalline material with precipitates. Example: nickel-based superalloy containing γ'-Ni_3Al precipitates. (h) Two-phase material after eutectoid transformation which represents the outcome of a diffusion-controlled reaction. The grains consist of alternating layers (or lamellae) of the constituting phases. The mechanical properties, for example, the yield strength, depend primarily on the lamellae spacing. Example: pearlitic steels.

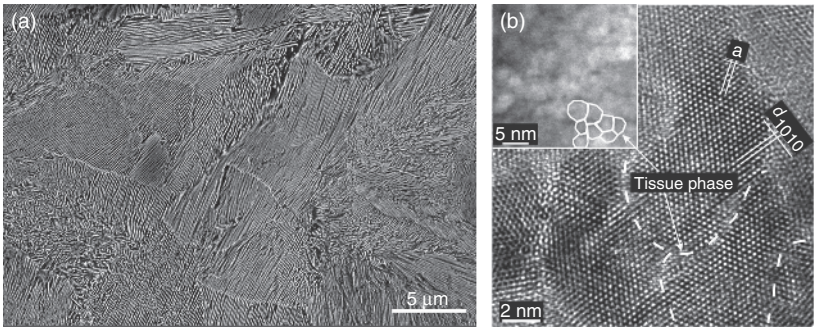

Figure 1.4 (a) "Conventional microstructure" of a pearlitic steel (scanning electron microscope image) and (b) "advanced nanostructure" of a superhard TiB_2 coating (high-resolution transmission electron microscope image). (Mayrhofer 2005 [15]. Reproduced with permission of Wiley.) The grain size of the pearlitic steel is about 10 µm, whereas the grain size of the TiB_2 coating is below 5 nm.

that is different to that existing in the deformed material. This type of texture is termed annealing or recrystallization texture (see Chapters 3, 10, and 18).

As examples for the described microstructures, Figure 1.4 displays images of a pearlitic steel and the nanostructure of a superhard TiB_2 coating. The grain size of the pearlitic steel is about 10 µm, whereas the grain size of the TiB_2 coating is below 5 nm. Today's advanced engineering metallic materials represent a combination of both features. For example, nickel-based superalloys, some aluminum alloys, and iron-based tool steels possess a "conventional" matrix with regard to grain size. The matrix, however, is hardened and strengthened by nanometer-sized and uniformly dispersed particles that precipitate from a supersaturated solid solution.

1.3 Microstructure and Properties

In the previous section it was pointed out that the properties of engineering metallic materials depend on the atomic arrangement, the prevailing crystal defects as well as the arrangement and morphology of the constituting phases/particles (see Figure 1.2 and Tables 1.1–1.3). In the following text, the influence of microstructural parameters on mechanical strength will be discussed. In general, the strength of a metal is controlled by the number and motion of dislocations. The stress required to move dislocations, the Peierls–Nabarro stress, is relatively low in pure metals. Consequently, in order to strengthen metals one must restrict the motion of dislocations by either generating internal stresses that oppose their motion, or by placing particles in their path that require them to cut or to loop the particles. Figure 1.5a,b summarizes the basic strengthening mechanisms for metallic materials at low ($T < 0.3T_M$) and high ($T > 0.3T_M$) temperatures. T_M is the melting point (in Kelvin) of the metal or alloy under consideration. Practically, there are four major strengthening mechanisms that will be outlined in the following: (1) work (dislocation density) hardening, (2) strengthening by grain size reduction, (3) solid solution strengthening, and (4) strengthening by particles.

1) The work hardening phenomenon can be explained on the basis of dislocation–dislocation strain field interactions. Plastic deformation during cold working

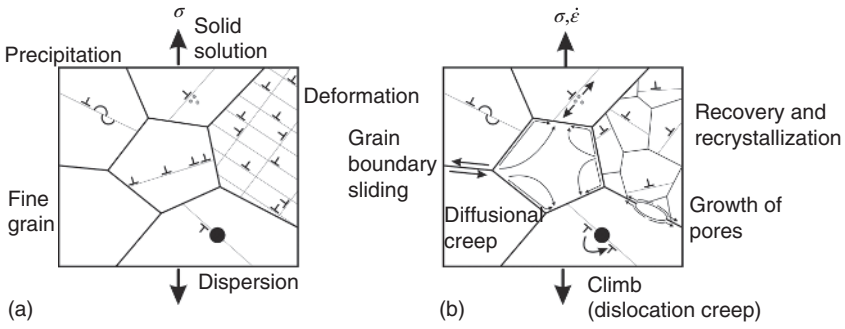

Figure 1.5 Basic strengthening mechanisms for metallic materials at low ($T < 0.3T_M$) and high ($T > 0.3T_M$) temperatures. T_M is the melting point in Kelvin. (a) At low temperatures the (yield) strength of a material is controlled by dislocation density (work hardening or strain hardening), grain size (grain boundary strengthening), concentration and size of alloying atoms (solid solution strengthening), and size and volume fraction of particles (precipitation or dispersion strengthening). (b) At high temperatures thermally activated processes and creep determine the occurring strength. For example, a high dislocation density is reduced by recovery and recrystallization. Fine-grained microstructures lead to high diffusion creep rates and pronounced grain boundary sliding. Particles that are effective barriers to dislocations at low temperatures are surmounted by climb processes (dislocation creep). Depending on the loading conditions, pores nucleate and grow at grain boundaries leading to micro- and macrostructural damage and consequently to a reduced lifetime.

produces an increase in the number of dislocations (Table 1.2). As a consequence, the mean distance between individual dislocations decreases. On average, dislocation–dislocation strain interactions are repulsive. The net result is that the motion of a dislocation is hindered by the presence of other dislocations. As the dislocation density increases with increasing degree of deformation, the resistance to dislocation motion becomes more pronounced.

2) The yield strength of a metal is almost universally observed to increase as the grain size decreases. The experimental data virtually always show a linear relationship between yield strength and the reciprocal value of the square root of the grain diameter. The strengthening effect produced by grain size reduction results from the blockage of dislocations by grain boundaries. Therefore, a fine-grained material is stronger than one that is coarse grained, since the former has a greater total grain boundary area to obstruct dislocation motion. Two reasons can be given why grain boundaries act as barriers to dislocation motion during plastic deformation: firstly, grains are of different crystallographic orientations. If a dislocation passes from one grain to another it will have to change its direction of motion. This process becomes more difficult as the misorientation between the grains increases. Secondly, the atomic disorder within a grain boundary region results in a discontinuity of slip planes from one grain into the other. Boundaries between two different phases are also barriers to dislocations. Such a behavior is utilized in the strengthening of complex multi-phase metallic materials.
3) Solid solution hardening is another effective technique to strengthen and harden metals. When a solute atom (alloying atom) dissolves in a solid metal it may act as an atomic-sized obstacle to dislocation motion. The strengthening effect depends on the nature of the interaction of the dislocation with the solute atoms. Usually, two general interactions are considered, one of a chemical nature and the other of an

elastic nature. The difference in chemical bonding between solute atoms and solvent atoms is reflected in the difference in their elastic shear moduli. This difference gives rise to a change in the dislocation–atom interaction. If the solute atom has a different size than that of the matrix atoms, then a misfit strain field is produced around the solute atom that interacts with the strain field of the dislocations.

4) Particles may be introduced into the matrix either by precipitation or powder metallurgical approaches (see Section 1.2). These particles will interact with the dislocations causing the dislocations either to cut through the particles or to loop them. It should be noted that particle cutting is restricted to particles that are coherent or at least semicoherent to the matrix. The degree of strengthening resulting from nanometer-sized particles depends on their distribution in the matrix (see Chapter 12). In addition to the shape, the second-phase dispersion can be described by specifying volume fraction, average particle diameter, and mean interparticle spacing.

At elevated temperatures ($T > 0.3T_M$), the microstructure may become thermally unstable (Figure 1.5b) and thermally activated processes such as diffusion and creep start determining the strength of the material. For example, a hardened cold-worked material can lose its strength due to recovery and recrystallization (see Chapter 17). Fine-grained materials that show good strength properties at ambient temperatures are prone to diffusional creep and pronounced grain boundary sliding. Furthermore, particles that are effective barriers to dislocations at low temperatures can be surmounted by diffusion-assisted climb processes (dislocation creep).

As a conclusion, Table 1.4 summarizes the discussed basic strengthening mechanisms and assesses their effect at low and high temperatures. It is worth mentioning here that the mechanical properties might not show the same size dependence when the grain sizes or the material dimensions reach the nanometer regime. This is most likely related to the difficulty to generate and move dislocations in these materials and ongoing research works are addressing this problem. The interested reader might find an introduction to this research field in [24–28].

1.4 Microstructural Characterization

As has been outlined in the previous sections, the microstructure has a major influence on the properties of engineering materials, and the most relevant microstructural features are summarized in Table 1.5. Usually, a combination of different characterization methods has to be applied to obtain the necessary information, and this section is devoted to this topic. However, only a rough guideline can be provided as to which methods can be applied to assess a specific microstructural feature, which may not be exhaustive. For a detailed description of the operating modes of the different methods the reader is referred to literature [7, 16–23] and to specific chapters of this book.

The most frequently used characterization techniques for studying the microstructure of engineering materials are light optical microscopy, electron and ion beam microscopy and corresponding analytical measurements as well as X-ray, neutron, and electron diffraction experiments. All of these methods are based on the elastic or inelastic interaction of a probe (visible light, electrons, ions, X-rays, neutrons) with the material under investigation giving rise to a scattered intensity of the initial beam and to the generation of secondary signals (photons, electrons, ions). Each method

Table 1.4 Basic strengthening mechanisms for engineering metallic materials and their assessment.

	Dislocations	Grain boundaries	Solute atoms	Particles	Transformation	Anisotropy	
Strengthening mechanism	Work hardening	Grain boundary hardening	Solid-solution hardening	Precipitation/ dispersion hardening	Transformation hardening, for example, martensitic transformation	Crystal (structure, texture)	Microstructure (fiber composites; directed grains; duplex microstructure)
Scaling parameters	Dislocation density	Grain size	Concentration of solute atoms	Particle size and volume fraction	Quenching rate, alloy composition	Crystal orientation, intensity of texture	Strength, orientation and volume fraction of fibers; grain orientation; deformation behavior of constituent phases
Assessment (after [14])							
Low-temperature strength	++	++	+	++	++	+	+
High-temperature strength (creep)	±[a)]	−	+	++	±[b)]	+	+

Impact on yield strength: ++ increases strongly
+ increases
− decreases.

a) + if dislocations are pinned by stable particles; − if recrystallization takes place during high-temperature application (creep).

b) + if martensitic structure is maintained.

Table 1.5 Information on microstructure needed.

- Grain/subgrain/domain size
- Crystal structure and chemistry of grains and particles
- Preferred grain orientation (texture)
- Three-dimensional arrangement of phases
- Phase transitions (onset, temperatures …)
- Size, shape, and volume fraction of particles (precipitates, dispersoids)
- Structure and type of appearing interfaces, segregation to interfaces
- Types of defects and defect density (pores, cracks …)
- Vacancy concentration and dislocation density
- Local/residual stresses
- Microstructural evolution during deformation and/or thermal treatment
- Nucleation and growth processes

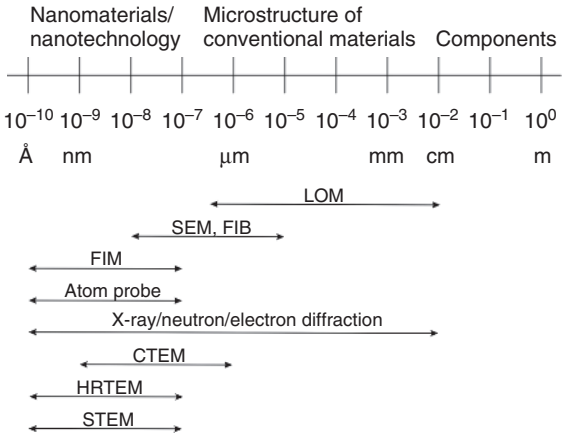

Figure 1.6 Length scale, which is covered in engineering materials, ranging from the atomic/nano scale to the dimensions of large components. Several characterization methods are listed as well as their resolution limits. LOM: light optical microscopy; SEM: scanning electron microscopy; FIB: focused ion beam; IM: ion microscopy; FIM: field ion microscopy; CTEM: conventional transmission electron microscopy; HRTEM: high resolution transmission electron microscopy; and STEM: scanning transmission electron microscopy.

allows the access of microstructural features on different length scales as indicated in Figure 1.6 and, except for X-ray and neutron diffraction techniques that will be addressed in the remaining chapters of this book, the others will be shortly described in the following text.

Light optical microscopy (LOM) is the common method that is employed to determine the grain size of engineering materials. In addition, the size and distribution of larger inclusions and precipitates can be investigated. However, due to a resolution limit in the order of the wavelength of light (i.e., around 500 nm) it is not suitable to investigate nanocrystalline materials or sub-micrometer precipitates. In addition, no information on the chemical composition or crystal structure of the individual phases can be obtained.

Scanning electron microscopy (SEM) and focused ion beam microscopy (FIB) enable us to study grain and precipitate sizes as well as their arrangement with a spatial resolution in the order of several ten nanometers. The resolution in the image is thereby mainly governed by the beam size. Often these microscopes are equipped with analytical

tools to perform energy-dispersive X-ray spectroscopy (EDX) and wavelength dispersive X-ray spectroscopy (WDX) (in the SEM) or secondary ion mass spectroscopy (SIMS) (in the FIB). These analytical methods can be used to determine the chemical composition of different phases. Since the interaction volume of the incident electron beam within the sample is much larger than the beam size (which can be as small as a few nanometers), semiquantitative EDX or WDX measurements can only be done with a resolution of about 1 μm. In principle, for SIMS a sub-micrometer lateral resolution can be achieved; however, in practice this resolution is often not obtained due to insufficient counting statistics. Thus, even if the size distribution of small particles can be determined, the classification of the corresponding particle types (regarding, e.g., chemical composition) is not possible and requires the use of an additional characterization method. Modern SEM are often equipped with an electron back scatter diffraction (EBSD) detector that allows to investigate the crystal structure of the occurring phases and their preferred orientation (texture) within the sample surface. The spatial resolution is in the range of 50 nm. An example of FIB/SEM tomography conducted on an intermetallic Ti-44 at.%Al-7 at.%Mo-0.1 at.%B alloy is depicted in Figure 1.7. The investigated alloy consists of two ordered phases, γ-TiAl ($L1_0$ structure) and β_o-TiAl (B_2 structure), which exhibit nearly the same volume fraction. Figure 1.7a,b shows the reconstruction of the γ- and β_o-phase, respectively. For both phases almost the whole volume is interconnected and forms a network. Specifics concerning the shown FIB/SEM tomography as well as 3D image analysis are reported in [29] and the references cited therein.

The crystal structure of sub-micrometer-sized particles and precipitates can be studied by transmission electron microscopy (TEM) using electron diffraction experiments. These studies can also be conducted to determine the orientation relationship between different phases or to show the presence of special grain boundaries such as twin boundaries. With the help of conventional TEM images (bright-field, dark-field, weak-beam) microstructural features such as dislocation densities, antiphase boundaries, grain/subgrain/domain sizes, particle shape, size, and distribution can be addressed. The spatial resolution for conventional TEM investigations is in the order of some nanometers. Figure 1.8a shows the presence of dislocations and mechanical twins

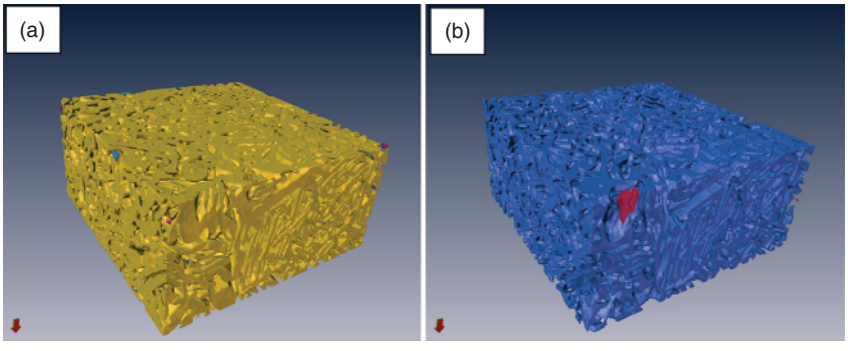

Figure 1.7 3D reconstruction of the constituting phases of an intermetallic Ti-44 at%Al-7 at.%Mo-0.1 at.%B alloy: (a) γ-TiAl and (b) β_o-TiAl. For both phases almost the whole volume is interconnected, except small particles at the border which are marked with different colors. The region of interest has an approximate size of $35 \times 17 \times 35\ \mu m^3$. (Engstler 2013 [29]. Reproduced with permission of Wiley.)

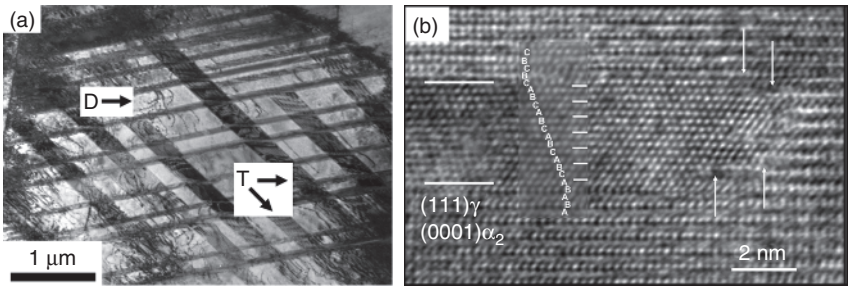

Figure 1.8 (a) TEM image of a Ti-46.5 at.%Al-4 at.% (Cr, Nb, Ta, B) sample deformed in compression up to 5% at room temperature reveals two different deformation mechanisms acting in γ-grains, mechanical (deformation) twinning (T) and dislocation glide (D). Note that cross-twinning with the primary twinning system limits the extension of the second twinning system. (Kauffmann 2000 [30]. Reproduced with permission of Elsevier.) (b) HRTEM image of a γ-TiAl lamella that terminates within the supersaturated α_2-Ti_3Al matrix in a Ti-45 at.%Al-7.5 at.%Nb specimen (Fischer 2010 [32]. Reproduced with permission of Elsevier.). The stacking sequence of the close packed planes is indicated. The $(111)\gamma//(0001)\alpha_2$ habit planes are marked by full lines. The arrows point to misfit dislocations. Beam direction = $[\bar{1}\,1\,0]\gamma||[\bar{1}\,\bar{2}\,\bar{1}\,0]\alpha_2$.

in a deformed γ-TiAl grain within a Ti-46.5 at.%Al-4 at.%(Cr, Nb, Ta, B) alloy. From the TEM image it is evident that in the observed γ-grain more than one twin system has been activated [30, 31].

Analytical TEM measurements such as EDX and electron energy-loss spectroscopy (EELS) allow to determine the chemical composition of individual phases, particles, or at interfaces. The spatial resolution of these methods depends strongly on the beam size, and for modern TEM with a scanning unit (scanning transmission electron microscopy (STEM)) a resolution of about 1 nm is achieved for EDX and ≥0.1 nm for EELS measurements. The main reason for the differences in resolution is attributed to the larger specimen thickness (and thus stronger effect of beam broadening within the sample) for EDX measurements (to obtain a better signal-to-noise ratio in the data) and due to the detection geometries.

The EELS measurements can be used not only to determine the chemical composition of the investigated region, but also to get an insight into the electronic structure. This is obtained by analyzing the electron energy-loss near-edge structure (ELNES) that is associated with each element-specific ionization edge and which contains information on, for example, bonding characteristics and nominal oxidation states of the probed atoms. In addition, studying the extended energy-loss fine structure (EXELFS), which occurs around 50 eV above the ionization edge onset, allows to obtain information on the radial distribution function of the atoms. The valence loss region with its characteristic plasmon features at an energy loss of around 15–25 eV can be used to investigate the optical properties of the materials by a subsequent Kramers–Kronig analysis. However, due to the nature of the excitation process these latter measurements can only be done with a spatial resolution of a few nanometers.

High-resolution transmission electron microscopy (HRTEM) and so-called *Z*-contrast images (*Z* stands for the atomic number) using a STEM allow to study the atomic structure of interfaces or the crystal structure of nanometer-sized precipitates.

The HRTEM image formation can be described with the help of Abbe's theory, and the image can be understood as an interference pattern of different diffracted beams. For the imaging a parallel beam is used, and the whole interference pattern is detected simultaneously. In contrast, for a *Z*-contrast image a convergent electron beam is used and scanned over the sample. At each position of the beam, the intensity of electrons scattered in large scattering angles is detected and the image is formed serial point by point. The detected signal is roughly proportional to the square of the atomic number. The *Z*-contrast image can be understood as a convolution of the specimen function (atomic columns) with the electron beam function. The resolution limit of both methods is mainly governed by the spherical aberration (C_s) of the electron lenses, that is, of the objective lens, which is most important for the imaging in HRTEM and of the condenser lens, which is responsible for the electron beam size in the case for *Z*-contrast imaging in the STEM. Recent developments of C_s correctors allow obtaining, for both methods, a spatial resolution of $\leq$0.1 nm. Figure 1.8b shows a high-resolution HRTEM image of an intermetallic Ti-45 at.%Al-7.5 at.%Nb alloy [32]. At first, the specimen was oil quenched from the single α-phase field region. In a second step, the sample, which consists of supersaturated α_2-Ti_3Al grains, was continuously heated to 790 °C at a rate of 20 °C min^{-1}, immediately followed by oil quenching. The image shows a γ-TiAl lath that terminates within a α_2-Ti_3Al grain. The beam direction is $[\bar{1}10]\gamma||[\bar{1}\bar{2}\bar{1}0]\alpha_2$ and, therefore, the $(111)\gamma||(0001)\alpha_2$ interfaces, indicated by solid lines, are edge on. The stacking sequence of the close packed planes is indicated. Some steps exist along this interface with a height corresponding to a $(111)\gamma$ lattice plane distance. At the terminating end of the γ-TiAl lath, the lattice mismatch between the γ-TiAl and the α_2-Ti_3Al phase can be compensated by transformation dislocations that have the Burgers vector of a Shockley partial dislocation and occur on every other close packed plane [32].

It is important to mention that all TEM images reveal a two-dimensional projection of the three-dimensional sample. This can cause problems, for example, if particle distributions are investigated, and thus complementary methods have to be applied. In addition, problems can occur if the sample thickness is too large since then small particles embedded in the matrix might become invisible. Dislocation densities can only be estimated up to 10^{15} m^{-2}, and other methods have then to be applied. In addition, the TEM specimen preparation has to be taken into account, and care has to be taken not to change the original structure or at least to minimize possible damaging effects. In addition, only a limited specimen volume is analyzed in TEM and, statistically, evaluations of microstructural features are time consuming. Therefore, integral methods that probe the features over a large sample volume and that are nondestructive (regarding the sample preparation) such as X-ray and neutron scattering should be performed in addition.

Another method to image lattice defects such as dislocations and grain boundaries at an atomic level is the field-ion microscope (FIM). A positive voltage is applied to a fine tip of the material of interest, which leads to the ionization of an imaging gas (e.g., He, Ne). The ions of the imaging gas are then radially accelerated to a fluorescent screen, which is at a negative potential. The image represents the geometry of the atomic arrangement of the terraces of the tip. Particles of a second phase might lead to a different ionization behavior of the imaging gas and thus appear differently. If the applied electrical field is

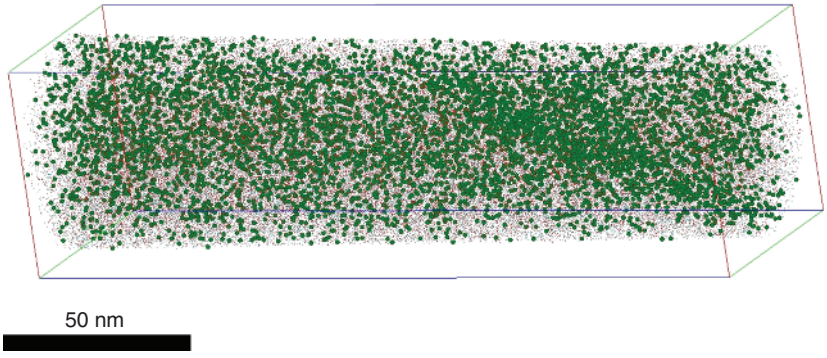

Figure 1.9 Atom probe image of C enrichment at a dislocation in the γ-TiAl-phase of an intermetallic Ti-45 at.%Al-5 at.%Nb-0.5 at.%C alloy. Every dot corresponds to a C atom. (Scheu 2009 [33]. Reproduced with permission of Elsevier.)

high enough, the atoms of the tip can be ionized themselves and leave the tip in radial directions. The ions can be identified with the help of a time-of-flight mass spectrometer, which is the basic working principle of an atom probe. A three-dimensional image of the tip can be obtained with suitable detectors. This method is especially suitable to study the initial stages of precipitations or to determine the chemical composition of impurity elements at defects such as dislocations or interfaces. As an example, Figure 1.9 illustrates the three-dimensional elemental distribution of C atoms within the γ-TiAl phase of a Ti-45 at.%Al-5 at.%Nb-0.5 at%C alloy. In the investigated Nb-containing alloy, C was found to be homogeneously distributed within the γ-TiAl-phase. Locally C enriched areas in the γ-TiAl-phase were found only at dislocations, forming so-called Cottrell atmospheres as described in [33]. More information with regard to intermetallic TiAl alloys and the contribution of synchrotron radiation and neutrons to their characterization and development is given in Chapter 22.

The tip preparation of samples containing defects can be rather time consuming, but using an FIB can help to produce a needle from the area of interest. However, not all materials can withstand the high electrical field and, as for the TEM investigations, the analyzed sample volume is rather small. Again, complementary methods are required to access the microstructural features governing the properties of engineering materials.

Despite the methods described so far, a variety of other imaging characterization techniques exist such as scanning probe microscopes, for example, scanning tunneling microscope and atomic force microscope [23]. These methods are helpful to get an insight into the surface structure of engineering materials down to the atomic level, but information on, for example, surface stresses on a larger scale are not easy to address. Since material scientists are generally interested to obtain all the information listed in Table 1.5 with a high statistical relevance, diffraction techniques are the right choice for microstructural characterization – if possible always linked to complementary methods such as the ones mentioned in this chapter. The following chapters will provide the basic background in the underlying physics of X-ray and neutron diffraction. In addition, the experimental setups used for the measurements are explained and fundamental descriptions of data treatment and analysis are given.

References

1 Shackelford, J.F. (2009) *Introduction to Materials Science for Engineers*, Pearson Education, New Jersey.
2 Verhoeven, J.D. (1994) *Fundamentals of Physical Metallurgy*, Wiley, Inc., New York.
3 Callister, W.D. (2011) *Materials Science and Engineering – An Introduction*, Wiley, New York, Weinheim.
4 Tetelman, A., Barrett, C.R., and Nix, W.D. (2005) *The Principles of Engineering Materials*, Prentice-Hall, Englewood Cliffs, NJ.
5 Weidmann, G., Lewis, P., and Reid, N. (1990) *Structural Materials*, Butterworth, London.
6 Gottstein, G. (2007) *Physikalische Grundlagen der Materialkunde*, Springer, Berlin.
7 Haasen, P. (2013) *Physikalische Metallkunde*, Springer, Berlin.
8 Cahn, R.W., Haasen, P., and Kramer, E.J. (eds) (2005) *Materials Science and Technology*, vol. **2a/2b, 6/7, 15/16**, Weinheim, Wiley-VCH Verlag GmbH.
9 Porter, D.A. and Easterling, K.E. (2009) *Transformations in Metals and Alloys*, Nelson Thornes, Cheltenham.
10 Hull, D. and Bacon, D.J. (2011) *Introduction to Dislocations*, Butterworth-Heinemann, Oxford.
11 Dieter, G.E. (1988) *Mechanical Metallurgy*, McGraw-Hill, London.
12 Smallman, R.E. and Bishop, R.J. (2014) *Modern Physical Metallurgy & Materials Engineering*, Butterworth-Heinemann, Oxford.
13 Courtney, T.H. (2013) *Mechanical Behavior of Materials*, McGraw-Hill, London.
14 Hornbogen, E. (1974) in *High-Temperature Materials in Gas Turbines* (eds P.R. Sahm and M.O. Speidel), Elsevier, Amsterdam, pp. 187–205.
15 Mayrhofer, P.H., Mitterer, C., and Clemens, H. (2005) Self-organized nanostructures in hard ceramic coatings. *Adv. Eng. Mater.*, **7**, 1071–1082.
16 Brandon, D. and Kaplan, W.D. (2008) *Microstructural Characterization of Materials*, John Wiley & Sons, Ltd., West Sussex.
17 Reimer, L. (1998) *Scanning Electron Microscopy*, Springer Series in Optical Sciences, 2nd edn, Springer, Berlin.
18 Williams, D.B. and Carter, C.B. (2011) *Transmission Electron Microscopy*, vol. **1–4**, Plenum Press, New York.
19 Fultz, B. and Howe, J.M. (2008) *Transmission Electron Microscopy and Diffractometry of Materials*, Springer, Berlin.
20 Reimer, L. (1997) *Transmission Electron Microscopy*, Springer Series in Optical Sciences, 4th edn, Springer, Berlin.
21 Miller, M.K., Cerezo, A., Hetherington, M.G., and Smith, G.D.W. (2006) *Atom Probe Field Ion Microscopy*, Oxford University Press, Oxford.
22 Hono, K. (2002) Nanoscale microstructural analysis of metallic materials by atom probe field ion microscopy. *Prog. Mater Sci.*, **46** (**6**), 621–729.
23 Brundle, C.R., Evans, C.A., and Wilson, S. (1992) *Encyclopedia of Materials Characterization – Surfaces, Interfaces, Thin Films*, Butterworth-Heinemann, Stoneham, MA.

24 Nix, W.D. (1989) Mechanical properties of thin films. *Metall. Trans. A*, **20** (**11**), 2217–2245.

25 Gleiter, H. (2000) Nanostructured materials: basic concepts and microstructure. *Acta Mater.*, **48** (**1**), 1–29.

26 Arzt, E., Dehm, G., Gumbsch, P., Kraft, O., and Weiss, D. (2001) Interface controlled plasticity in metals: dispersion hardening and thin film deformation. *Prog. Mater Sci.*, **46** (**3–4**), 283–307.

27 Freund, L.B. and Suresh, S. (2004) *Thin Film Materials: Stress, Defect Formation and Surface Evolution*, Cambridge University Press, Cambridge.

28 Dehm, G., Motz, C., Scheu, C., Clemens, H., Mayrhofer, P., and Mitterer, C. (2006) Mechanical size-effects in miniaturized and bulk materials. *Adv. Eng. Mater.*, **8**, 1033–1045.

29 Engstler, M., Mayer, S., Pauly, C., Clemens, H., and Mücklich, F. (2013) 3D characterization of an intermetallic β/γ-titanium aluminide alloy. *Adv. Eng. Mater.*, **15**, 1125–1128.

30 Kauffmann, F., Bidlingmaier, T., Dehm, G., Wanner, A., and Clemens, H. (2000) On the origin of acoustic emission during room temperature compressive deformation of a γ-TiAl based alloy. *Intermetallics*, **8**, 823–830.

31 Clemens, H. and Mayer, S. (2013) Design, processing, microstructure, properties, and applications of advanced intermetallic TiAl alloys 2013. *Adv. Eng. Mater.*, **15**, 191–215.

32 Fischer, F.D., Waitz, T., Scheu, C., Cha, L., Dehm, G., Antretter, T., and Clemens, H. (2010) Study of nanometer-scaled lamellar microstructure in a Ti-45Al-7.5Nb alloy – experiments and modelling. *Intermetallics*, **18**, 509–517.

33 Scheu, C., Stergar, E., Schober, M., Cha, L., Clemens, H., Bartels, A., Schimansky, F.-P., and Cerezo, A. (2009) High carbon solubility of a γ-TiAl based Ti-45Al-5Nb-0.5C alloy and its effect on hardening. *Acta Mater.*, **57**, 1504–1511.